

Excitation functions of parameters extracted from three-source (net-)proton rapidity distributions in Au-Au and Pb-Pb collisions over an energy range from AGS to RHIC

Li-Na Gao^a, Fu-Hu Liu^{a,1}, Yan Sun^b, Zhu Sun^b, Roy A. Lacey^c,

^a*Institute of Theoretical Physics, Shanxi University, Taiyuan, Shanxi 030006, China*

^b*Department of Physics, Shanxi Datong University, Datong, Shanxi 037009, China*

^c*Departments of Chemistry & Physics, Stony Brook University, Stony Brook, NY 11794, USA*

Abstract: Experimental results of the rapidity spectra of protons and net-protons (protons minus antiprotons) emitted in gold-gold (Au-Au) and lead-lead (Pb-Pb) collisions, measured by a few collaborations at the alternating gradient synchrotron (AGS), super proton synchrotron (SPS), and relativistic heavy ion collider (RHIC), are described by a three-source distribution. The values of the distribution width σ_C and fraction k_C of the central rapidity region, and the distribution width σ_F and rapidity shift Δy of the forward/backward rapidity regions, are then obtained. The excitation function of σ_C increases generally with increase of the center-of-mass energy per nucleon pair $\sqrt{s_{NN}}$. The excitation function of σ_F shows a saturation at $\sqrt{s_{NN}} = 8.8$ GeV. The excitation function of k_C shows a minimum at $\sqrt{s_{NN}} = 8.8$ GeV and a saturation at $\sqrt{s_{NN}} \approx 17$ GeV. The excitation function of Δy increases linearly with $\ln(\sqrt{s_{NN}})$ in the considered energy range.

Keywords: Rapidity distribution of (net-)protons, three-source distribution, excitation functions of parameters, minimum, softest point

PACS: 13.85.-t, 13.85.Ni, 25.75.Dw, 24.10.Nz, 24.10.Pa

1 Introduction

Rapidity (or pseudorapidity) distributions of charged particles produced in nucleus-nucleus (heavy ion) collisions at high energies are an important topic measured in experiments and analyzed in theories [1–3]. In particular, the rapidity distributions of protons and net-protons (protons minus antiprotons, i.e. $p - \bar{p}$) are related to not only the energy loss or stopping power of colliding nuclei but also the number density and mean free path of the considered particles, which are related to the onset of deconfinement in high energy nucleus-nucleus collisions [4–6]. This energy loss of colliding nuclei is also a fundamental quantity which determines the effective energy available for production yields of particles and excitation degree of interacting system [7]. This effective energy is essential for the formation of a deconfined quark and gluon phase of matter, i.e. quark-gluon plasma (QGP) or quark matter. To determine the critical energy of phase transition from hadronic matter to QGP is an important and difficult topic [8]. Before making a

¹E-mail: fuhuliu@163.com; fuhuliu@sxu.edu.cn

determination, one needs to search for some softest points in the equation of state (EoS), which should be relative to the local minimums in some excitation functions which are the dependences of parameters on collision energy.

The width and peak (or hollow) position of rapidity distribution are very sensitive quantities which are related to collision energy, in particular for peak (or hollow) position in the laboratory reference frame. It is expected that the system at different collision energies corresponds to different interacting mechanisms. In nucleus-nucleus collisions over an energy range from the alternating gradient synchrotron (AGS) to super proton synchrotron (SPS) and relativistic heavy ion collider (RHIC), the interacting system undergoes the liquid-like state of nucleon matter, gas-like state of hadronic matter, and liquid-like state of quark matter. From AGS to RHIC, it is expected that the excitation functions of the mentioned parameters should experience a minimum or other change due to the interacting system changing from liquid-like state to gas-like state and then liquid-like state again, though the two liquid-like states correspond to different types of matters.

Although we can simply and approximately use a Gaussian function to fit rapidity distributions in some cases, two or more Gaussian functions can give better descriptions. In fact, in most cases, the experimental rapidity spectra cannot be exactly described by a single Gaussian function [9, 10]. Instead, we need two or three Gaussian functions to describe the experimental spectra. In the case of using a two-Gaussian function [9, 10], the first and second functions correspond to the contributions of the forward and backward (or backward and forward) rapidity regions respectively. In the case of using a three-Gaussian function, the third function is regarded as the contribution of the central rapidity region [4–6, 11–13]. Since the two-source is possibly misunderstood by the false appearance which implies an unbelievable case that there is no source in the central rapidity region, we would rather use the three-source distribution [4–6, 11–13] than the two-source one, though the former has more parameters than the latter.

Although the three-source distribution has been used in our previous works [14–16], in which the rapidity distributions of charged particles, which are mainly charged pions, produced in proton-proton and nucleus-nucleus collisions were reported, the present work focusses on the rapidity spectra of (net-)protons emitted in gold-gold (Au-Au) and lead-lead (Pb-Pb) collisions over an energy range from AGS to RHIC. It is expected that some minimums and other phenomenons in the excitation functions of parameters extracted from the rapidity spectra of (net-)protons should be observed.

The rest of this paper is structured as follows. The model and formalism are shortly described in section 2. Results and discussion are given in section 3. In section 4, we summarize our main observations and conclusions.

2 The model and formalism

As introduced above, we would like to use three Gaussian functions [14–16] to fit the rapidity spectra of charged particles produced in nucleus-nucleus collisions at high energies, where the charged particles are mainly charged pions, and include also protons and others. The three Gaussian functions cater to the three-source model [4–6, 11–13].

Although the three-source distribution uses more parameters than the two-source one, the former should give a better description than the latter.

Based on the focus of the present work and the three-source distribution [4–6, 14–16], we assume the rapidity distribution, dN/dy , of (net-)protons emitted in symmetric nucleus-nucleus collisions at high energies to be

$$\begin{aligned} \frac{dN}{dy} = & \frac{N_0}{\sqrt{2\pi}} \left\{ \frac{1 - k_C}{2\sigma_F} \exp \left[- \frac{(y - y_{cm} + \Delta y)^2}{2\sigma_F^2} \right] \right. \\ & + \frac{k_C}{\sigma_C} \exp \left[- \frac{(y - y_{cm})^2}{2\sigma_C^2} \right] \\ & \left. + \frac{1 - k_C}{2\sigma_F} \exp \left[- \frac{(y - y_{cm} - \Delta y)^2}{2\sigma_F^2} \right] \right\}, \end{aligned} \quad (1)$$

where y_{cm} denotes the mid-rapidity or the rapidity of the center-of-mass, and $y_{cm} = 0$ for symmetric collisions in the center-of-mass reference frame; σ_C and k_C denote the rapidity distribution width and fraction of the central rapidity region, respectively; σ_F and Δy denote the rapidity distribution width and rapidity shift (peak position) of the forward/backward rapidity regions, respectively; and N_0 denotes the normalization constant when we compare the normalized distribution to the experimental spectrum. In the present work, y and $y - y_{cm}$ are in fact the rapidities in the laboratory and center-of-mass reference frames, respectively.

We have four main parameters, σ_C , σ_F , k_C , and Δy , in the above discussion. The selections of the four main parameters are influenced each other in the fitting process. To determine the best values of parameters, we have used the method of least squares. The minimum χ^2 corresponds to the best values of parameters. An appropriate increase in χ^2 determines the uncertainties of parameters when we increase or decrease some amounts in the best values of parameters. By analyzing experimental data in nucleus-nucleus collisions over an energy range from AGS to RHIC as much as possible, we can obtain the excitation functions of the four parameters in the considered energy range. At the same time, the dependences of parameters on collision centrality can be incidentally studied.

3 Results and discussion

Figures 1–3 present the rapidity distributions of protons emitted in Au-Au collisions at $\sqrt{s_{NN}} = 3.6, 4.1$, and 4.7 GeV, respectively. From panels (a) to (e), the corresponding centrality intervals are 0–5%, 5–12%, 12–23%, 23–39%, and 39–81%, respectively. The closed circles represent the experimental data of the E917 Collaboration [17] and the open circles are reflected at the mid-rapidity (with $y - y_{cm} = 0$). The curves are our results fitted by the three-source distribution. The values of free parameters σ_C , σ_F , k_C , and Δy , as well as the normalization constant N_0 are listed in Table 1 with the values of χ^2 per degree of freedom (dof). One can see that the model describes approximately the considered experimental data in most cases.

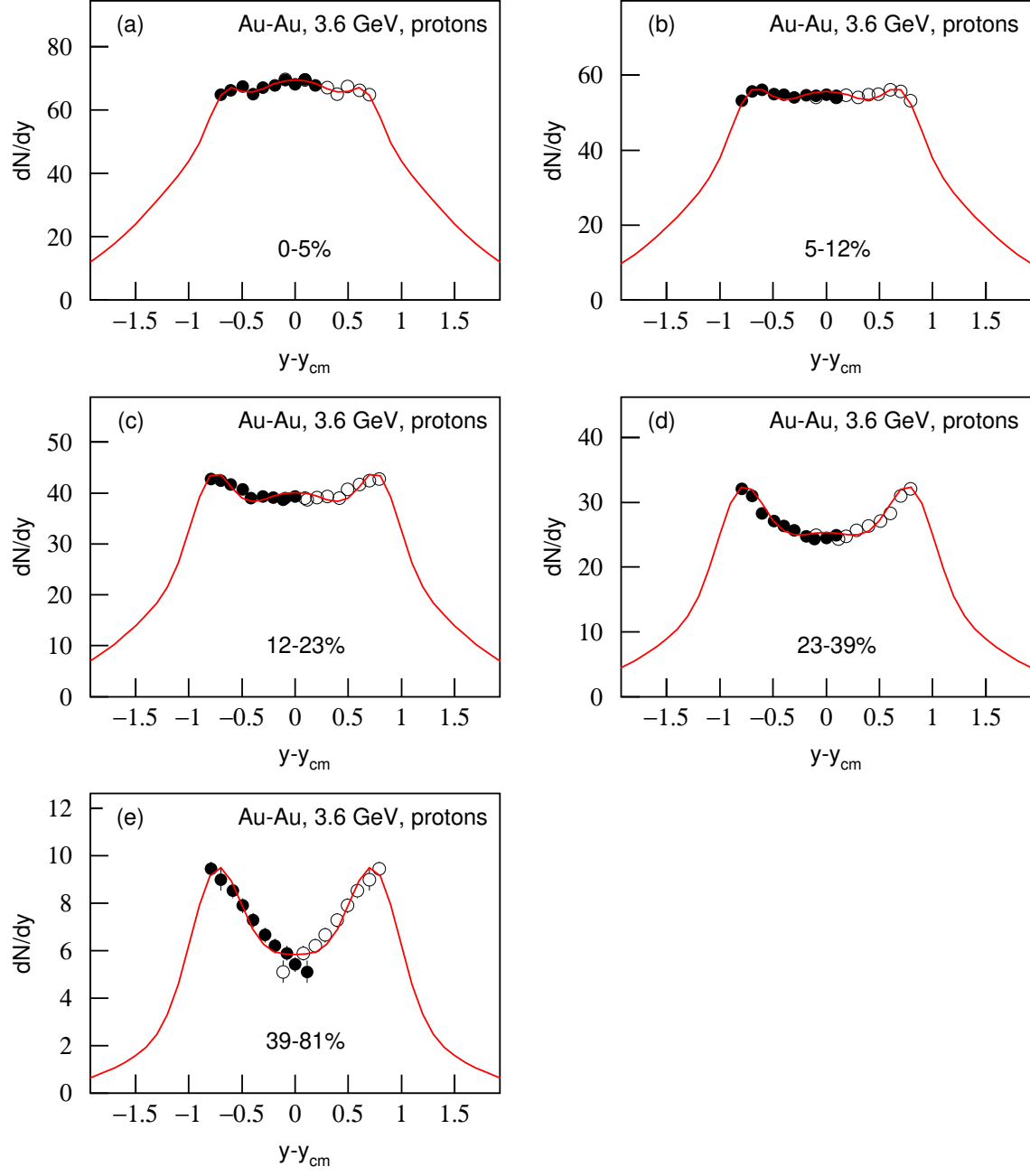


Figure 1. Rapidity distributions of protons emitted in Au-Au collisions at $\sqrt{s_{NN}} = 3.6$ GeV, where panels (a)–(e) correspond to centrality intervals 0–5%, 5–12%, 12–23%, 23–39%, and 39–81%, respectively. The closed circles represent the experimental data of the E917 Collaboration [17] and the open circles are reflected at the mid-rapidity. The curves are our results fitted by the three-source distribution.

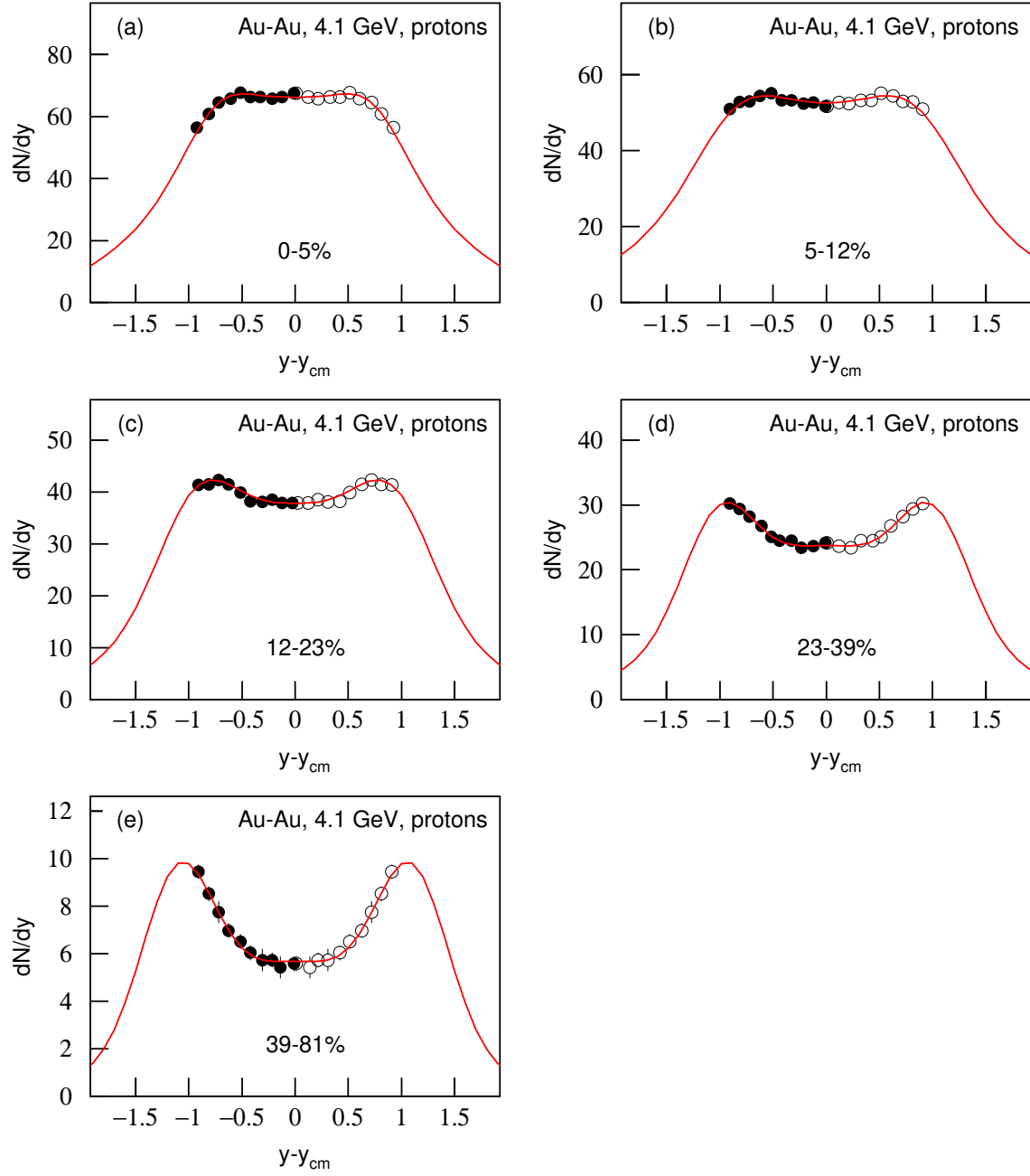


Figure 2. The same as Figure 1, but showing the results at $\sqrt{s_{NN}} = 4.1$ GeV.

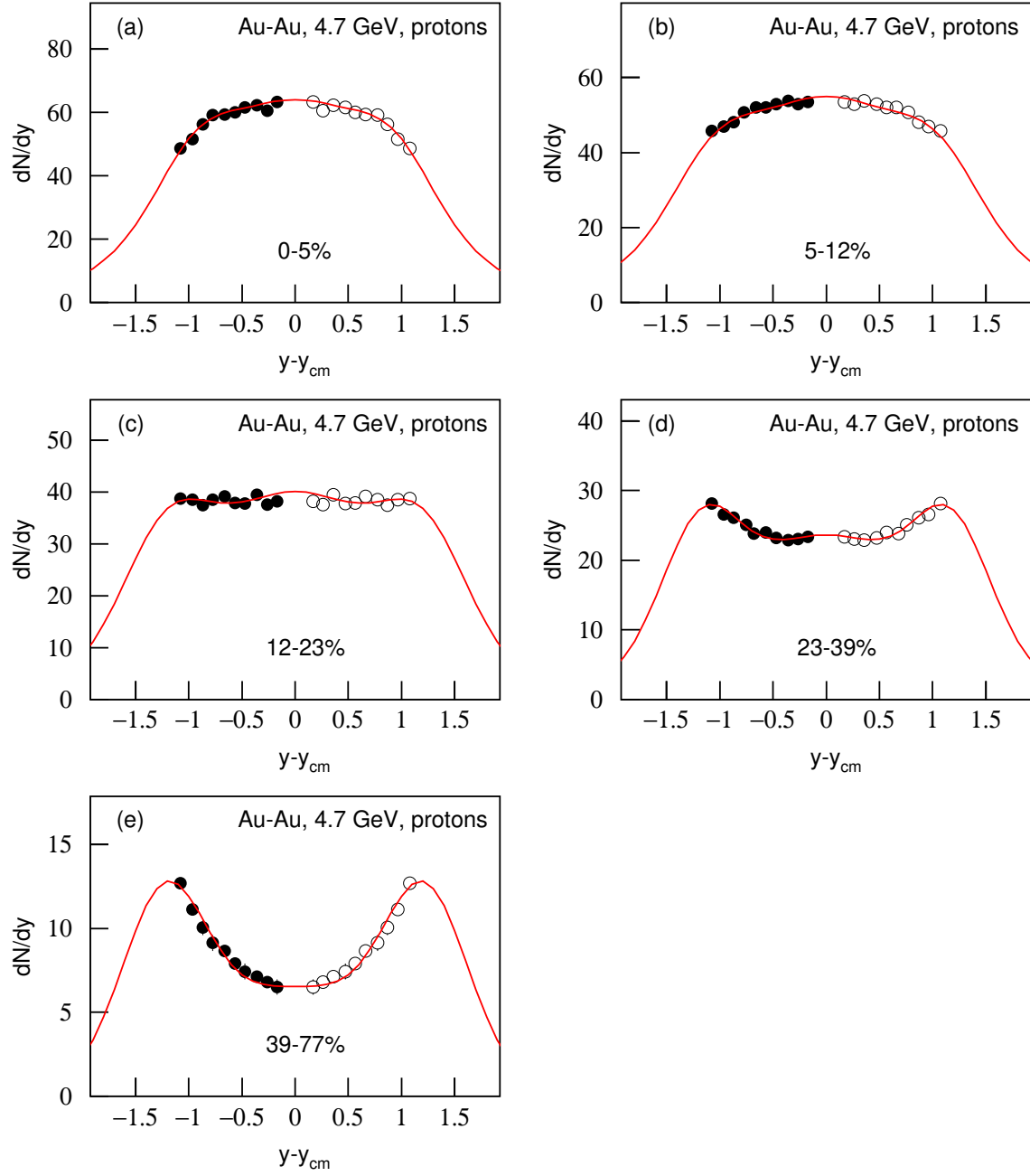


Figure 3. The same as Figure 1, but showing the results at $\sqrt{s_{NN}} = 4.7$ GeV.

Table 1. Values of free parameters, normalization constants, and χ^2/dof corresponding to the curves in Figures 1–7, where Figures 5(b), 6, and 7 correspond to Pb-Pb collisions, and others correspond to Au-Au collisions.

Figure	$\sqrt{s_{NN}}$ (GeV)	Centrality (%)	Particle	σ_C	σ_F	k_C	Δy	N_0	χ^2/dof
1(a)	3.6	0–5	p	1.030 ± 0.017	0.133 ± 0.007	0.965 ± 0.010	0.674 ± 0.036	186.2 ± 0.8	0.579
1(b)	3.6	5–12	p	1.032 ± 0.015	0.166 ± 0.008	0.935 ± 0.008	0.726 ± 0.024	154.3 ± 0.6	1.150
1(c)	3.6	12–23	p	1.031 ± 0.015	0.180 ± 0.010	0.893 ± 0.006	0.802 ± 0.030	116.2 ± 0.8	2.838
1(d)	3.6	23–39	p	1.033 ± 0.013	0.213 ± 0.008	0.818 ± 0.012	0.812 ± 0.030	80.1 ± 0.5	3.562
1(e)	3.6	39–81	p	0.923 ± 0.024	0.232 ± 0.012	0.685 ± 0.015	0.753 ± 0.054	19.5 ± 0.1	1.422
2(a)	4.1	0–5	p	1.043 ± 0.018	0.300 ± 0.011	0.895 ± 0.012	0.752 ± 0.066	190.1 ± 1.8	0.561
2(b)	4.1	5–12	p	1.148 ± 0.023	0.378 ± 0.015	0.854 ± 0.018	0.858 ± 0.084	170.3 ± 1.2	0.573
2(c)	4.1	12–23	p	1.025 ± 0.020	0.352 ± 0.012	0.765 ± 0.010	0.950 ± 0.090	124.2 ± 1.0	0.488
2(d)	4.1	23–39	p	1.038 ± 0.022	0.323 ± 0.013	0.711 ± 0.008	1.026 ± 0.024	86.2 ± 0.8	0.812
2(e)	4.1	39–81	p	1.024 ± 0.024	0.333 ± 0.013	0.565 ± 0.008	1.110 ± 0.066	25.5 ± 0.1	0.146
3(a)	4.7	0–5	p	1.002 ± 0.023	0.338 ± 0.017	0.878 ± 0.010	0.966 ± 0.066	182.4 ± 1.2	0.820
3(b)	4.7	5–12	p	1.042 ± 0.018	0.362 ± 0.013	0.865 ± 0.007	1.088 ± 0.084	165.2 ± 1.0	1.072
3(c)	4.7	12–23	p	1.024 ± 0.021	0.387 ± 0.010	0.758 ± 0.012	1.242 ± 0.060	135.2 ± 1.0	2.049
3(d)	4.7	23–39	p	1.006 ± 0.016	0.353 ± 0.007	0.682 ± 0.008	1.198 ± 0.066	87.1 ± 0.7	0.649
3(e)	4.7	39–77	p	1.005 ± 0.018	0.387 ± 0.013	0.462 ± 0.008	1.240 ± 0.054	35.0 ± 0.5	1.441
4(a)	2.4	0–5	p	0.583 ± 0.008	0.079 ± 0.006	0.989 ± 0.006	0.295 ± 0.042	118.3 ± 1.3	1.577
4(b)	3.1	0–5	p	0.775 ± 0.015	0.123 ± 0.010	0.993 ± 0.008	0.612 ± 0.036	141.7 ± 1.0	1.381
4(c)	3.6	0–5	p	0.966 ± 0.018	0.133 ± 0.012	0.992 ± 0.007	0.798 ± 0.033	152.5 ± 0.8	2.258
4(d)	4.1	0–5	p	0.978 ± 0.016	0.130 ± 0.014	0.990 ± 0.008	0.809 ± 0.033	152.2 ± 1.1	0.570
5(a)	5	0–5	$p - \bar{p}$	0.828 ± 0.027	0.288 ± 0.015	0.850 ± 0.016	0.903 ± 0.060	154.5 ± 1.2	1.088
5(b)	17.3	0–5	$p - \bar{p}$	1.718 ± 0.044	0.685 ± 0.034	0.603 ± 0.013	1.393 ± 0.069	162.7 ± 1.5	0.431
5(c)	200	0–5	$p - \bar{p}$	2.402 ± 0.068	0.727 ± 0.041	0.552 ± 0.010	2.580 ± 0.078	78.1 ± 0.7	0.171
5(d)	200	0–5	p	2.255 ± 0.072	0.500 ± 0.030	0.866 ± 0.014	2.450 ± 0.066	171.5 ± 1.1	0.042
6(a)	8.8	0–5	p	0.997 ± 0.027	0.596 ± 0.016	0.541 ± 0.011	1.166 ± 0.078	149.3 ± 0.9	0.215
6(b)	8.8	5–12.5	p	1.125 ± 0.030	0.736 ± 0.012	0.350 ± 0.013	1.126 ± 0.078	130.5 ± 1.0	2.536
6(c)	8.8	12.5–23.5	p	1.129 ± 0.029	0.722 ± 0.022	0.457 ± 0.010	1.533 ± 0.069	111.2 ± 0.8	0.413
6(d)	8.8	23.5–33.5	p	1.070 ± 0.030	0.655 ± 0.025	0.360 ± 0.015	1.682 ± 0.072	87.2 ± 0.8	1.384
6(e)	8.8	33.5–43.5	p	1.068 ± 0.028	0.605 ± 0.017	0.340 ± 0.012	1.652 ± 0.066	62.1 ± 0.7	0.945
7(a)	16.8	0–5	$p - \bar{p}$	1.796 ± 0.056	0.390 ± 0.020	0.762 ± 0.013	1.564 ± 0.072	165.8 ± 1.2	2.236
7(b)	16.8	5–12.5	$p - \bar{p}$	1.853 ± 0.050	0.524 ± 0.024	0.708 ± 0.018	1.722 ± 0.066	143.2 ± 1.2	1.136
7(c)	16.8	12.5–23.5	$p - \bar{p}$	1.778 ± 0.053	0.483 ± 0.017	0.717 ± 0.010	1.506 ± 0.078	91.1 ± 1.0	0.442
7(d)	16.8	23.5–33.5	$p - \bar{p}$	1.743 ± 0.047	0.523 ± 0.017	0.592 ± 0.015	1.744 ± 0.078	70.3 ± 0.3	2.014
7(e)	16.8	33.5–43.5	$p - \bar{p}$	1.730 ± 0.050	0.562 ± 0.018	0.562 ± 0.012	1.766 ± 0.072	46.2 ± 0.4	0.094

Figures 4 and 5 are the same as Figure 1, but they show the results of protons [Figures 4 and 5(d)] and net-protons [Figures 5(a)–5(c)] emitted in 0–5% Au-Au collisions over a $\sqrt{s_{NN}}$ range from 2.4 to 200 GeV, where the specific energies are marked in the panels. The closed circles represent the experimental data of the E895 [18], E802/E877/E917, NA49, and BRAHMS Collaborations [7, 19], and the open circles are reflected at the mid-rapidity. The curves are our results fitted by the three-source distribution. The values of free parameters σ_C , σ_F , k_C , and Δy , as well as the normalization constant N_0 are listed in Table 1 with the values of χ^2/dof . One can see that the model describes approximately the considered experimental data in most cases.

Figures 6 and 7 are similar to Figure 1, but they show the results of protons and net-protons emitted in Pb-Pb collisions at $\sqrt{s_{NN}} = 8.8$ and 16.8 GeV, respectively. From panels (a) to (d), the corresponding centrality intervals are 0–5%, 5–12.5%, 12.5–23.5%, and 23.5–33.5%, respectively. The closed circles represent the experimental data of the NA49 Collaboration [20] and the open circles are reflected at the mid-rapidity. The curves are our results fitted by the three-source distribution. The values of σ_C , σ_F , k_C , Δy , N_0 , and χ^2/dof are listed in Table 1. One can see that the model describes approximately the considered experimental data in most cases.

We notice that there are differences between the rapidity distributions of protons and net-protons. For instance, the data in Figures 5(c) and 5(d) are obviously different from each other. If the contributions of leading protons are excluded, the rapidity distribution shapes of protons and antiprotons are similar [21, 22], and they have the same rules as a function of the collision energy and centrality. Including the contributions of leading protons in the rapidity distribution of protons, two peaks appear in the forward and backward rapidity regions respectively, which is obviously different from those of antiprotons. As a result of protons minus antiprotons, the rapidity distribution of net-protons shows

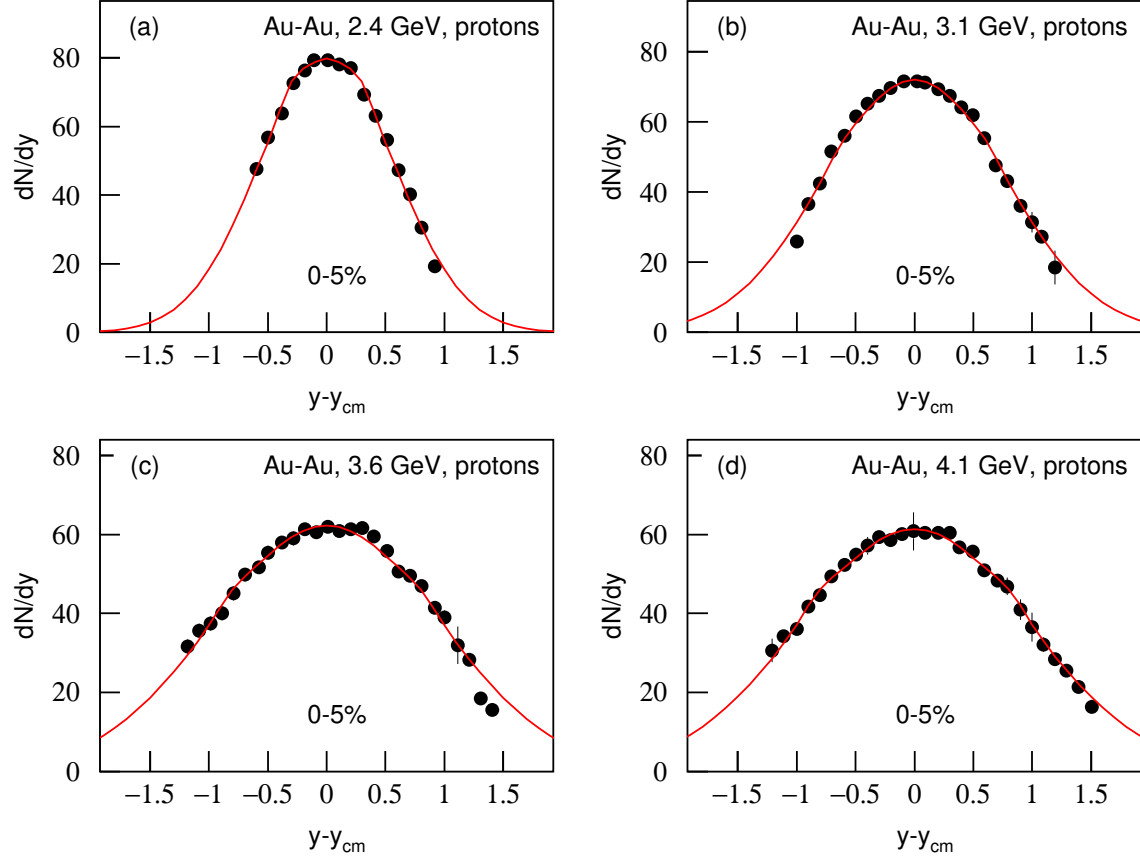


Figure 4. Rapidity distributions of protons emitted in 0-5% Au-Au collisions at $\sqrt{s_{NN}}$ being (a) 2.4, (b) 3.1, (c) 3.6, and (d) 4.1 GeV, respectively. The closed circles represent the experimental data of the E895 Collaboration [18]. The curves are our results fitted by the three-source distribution.

large differences from that of protons in all rapidity regions, particularly in very central and middle forward/backward rapidity regions.

As for the collisions which have the same collision energy and centrality, we can explain the differences by the statistical fluctuations and distribution ranges. In particular, the differences between Figures 4(c) and 1(a), as well as Figures 4(d) and 2(a), could be caused by the statistical fluctuations in different experiments measured by different collaborations in different rapidity ranges [17, 18]. In our opinion, to give a good enough description, one should use a wide enough rapidity distribution. The rapidity range of the E895 data presented in Figure 4 is wider than that of the E917 data presented in Figures 1–3. We are inclined to think that the description for Figure 4 is more accurate. In fact, we expect to describe the data in the whole rapidity range. Although emulsion experiment can satisfy this expectation, it is difficult to identify different particles and to give high statistics.

To study the excitation functions of free parameters, the left panel of Figure 8 shows the dependences of (a) σ_C , (c) σ_F , (e) k_C , and (g) Δy on $\sqrt{s_{NN}}$, respectively. The closed and open symbols represent parameter values from protons and net-protons respectively, and different symbols are for different centrality intervals shown in the panel. All parameter values are extracted from Figures 1–7 and listed in Table 1. It should be noticed that the error bars look very small due to all the four parameters being very sensitive quantities for rapidity distribution. A very small increase or decrease in the parameter values can cause a large dispersion from the expectation. To obtain a reasonable fitting result, we have to limit the parameters in very small ranges. The line segments in Figures 8(a) and 8(c) for central collisions are used to guide the eyes. Only the results for central collisions are presented in Figures 8(e) and 8(g) for the purpose of clarity and concision, where the solid and dashed lines in Figure 8(g) are our results fitted by the linear functions

$$\Delta y = (0.080 \pm 0.021) + (0.470 \pm 0.067) \ln(\sqrt{s_{NN}}) \quad (2)$$

with $\chi^2/\text{dof}=6.862$ and

$$\Delta y = (0.095 \pm 0.027) + (0.483 \pm 0.060) \ln(\sqrt{s_{NN}}) \quad (3)$$

with $\chi^2/\text{dof}=2.324$ respectively.

In the case of considering protons and net-protons together, from the left panel of Figure 8 one can see that σ_C increases generally with increase of $\sqrt{s_{NN}}$. At the same time, σ_F increases initially with increase of $\sqrt{s_{NN}}$ and then saturates at above 8.8 GeV and fluctuates around its value at 17 GeV. As the parameter described the fraction of the central rapidity region, k_C seems to show a confused energy dependence. In fact, k_C is related to other parameters which depend on energy. A careful observation shows a tendency that, with increasing $\sqrt{s_{NN}}$, k_C decreases quickly from 0.98 at 2.1 GeV to 0.55 at 8.8 GeV, and saturates to about 0.70 at above 17 GeV. This renders that k_C has a minimum at $\sqrt{s_{NN}} = 8.8$ GeV. In our considered energy range, Δy increases linearly with increase of $\ln(\sqrt{s_{NN}})$. Our observation shows the protons and net-protons having consistent results in most cases.

The characteristics of the excitation functions have some possible reasons. The trend of general increase in σ_C renders a continuous expansion of the central rapidity region in the considered energy range. The saturation of σ_F at $\sqrt{s_{NN}} > 8.8$ GeV renders the

scaling law and nuclear limiting fragmentation in the forward/backward rapidity regions. The saturation of k_C at $\sqrt{s_{NN}} > 17$ GeV renders that the number of non-leading protons which stay in the central rapidity region are independent of energy at higher AGS and RHIC energies, and the scaling law and nuclear limiting fragmentation appear again. The linear increase in Δy reflects the power of nuclear penetration which also increases with increase of $\ln(\sqrt{s_{NN}})$.

To study the relations of free parameters and the collision centrality C , the right panel of Figure 8 shows the dependences of (b) σ_C , (d) σ_F , (f) k_C , and (h) Δy on C , respectively. The closed and open symbols represent parameter values for protons and net-protons respectively, and different symbols are for different energies shown in the panel, which are extracted from Figures 1–7 and listed in Table 1. As mentioned in the above paragraph on the left panel of Figure 8, because all the four parameters are very sensitive quantities for rapidity distribution, they show very small error bars. The lines in Figures 8(b), 8(d), and 8(f) are our results fitted by a linear function, though some of them do not sure obey the linear relation. The corresponding intercepts and slopes are listed in Table 2 with χ^2/dof , where we see a few large χ^2/dof which imply a non-linear relation. The line segments in Figure 8(h) are used to guide the eyes.

One can see from the right panel of Figure 8 that, for the considered five energies, σ_C and σ_F have a slight change or do not change with decrease of the centrality (or increase of the centrality percentage). With decrease of the centrality, k_C decreases conformably for the five energies, and Δy increases for the energies at or near the minimum and does not change obviously for the energies apart from the minimum.

Table 2. Values of intercept, slope, and χ^2/dof corresponding to the lines in Figures 8(b), 8(d), and 8(f).

Figure	Relation	$\sqrt{s_{NN}}$ (GeV)	Intercept	Slope	χ^2/dof
8(b)	$\sigma_C - C$	3.6	1.054 ± 0.016	-0.002 ± 0.001	3.466
		4.1	1.081 ± 0.032	-0.001 ± 0.001	6.190
		4.7	1.023 ± 0.011	-0.001 ± 0.001	0.842
		8.8	1.066 ± 0.042	0.001 ± 0.001	4.674
		16.8	1.833 ± 0.022	-0.003 ± 0.001	0.380
8(d)	$\sigma_F - C$	3.6	0.147 ± 0.010	0.002 ± 0.001	4.127
		4.1	0.339 ± 0.020	-0.001 ± 0.001	7.344
		4.7	0.352 ± 0.012	0.001 ± 0.001	4.353
		8.8	0.683 ± 0.050	-0.001 ± 0.002	22.138
		16.8	0.428 ± 0.032	0.004 ± 0.001	4.415
8(f)	$k_C - C$	3.6	0.976 ± 0.003	-0.005 ± 0.001	0.167
		4.1	0.892 ± 0.013	-0.006 ± 0.001	4.322
		4.7	0.909 ± 0.011	-0.008 ± 0.001	4.794
		8.8	0.487 ± 0.051	-0.004 ± 0.002	38.062
		16.8	0.777 ± 0.021	-0.006 ± 0.001	7.063

The characteristics of the dependences of parameters on the centrality imply some possible reasons. The near independences of σ_C (σ_F) and partly Δy from C render that

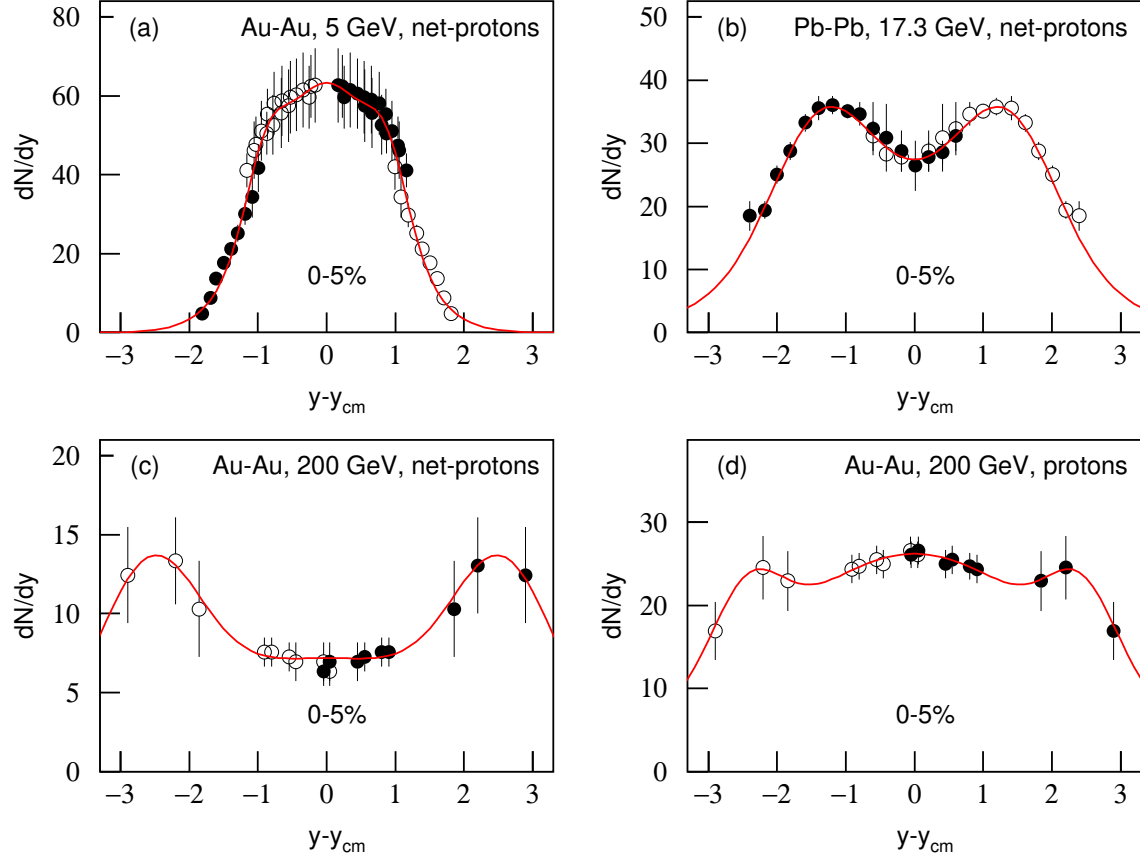


Figure 5. The same as Figure 4, but showing the results of (a)–(c) net-protons and (d) protons emitted in 0–5% Au-Au collisions at $\sqrt{s_{NN}}$ being (a) 5, (b) 17.3, and (c)(d) 200 GeV, respectively. The closed circles represent the experimental data of the E802/E877/E917, NA49, and BRAHMS Collaborations [7, 19] and the open circles are reflected at the mid-rapidity.

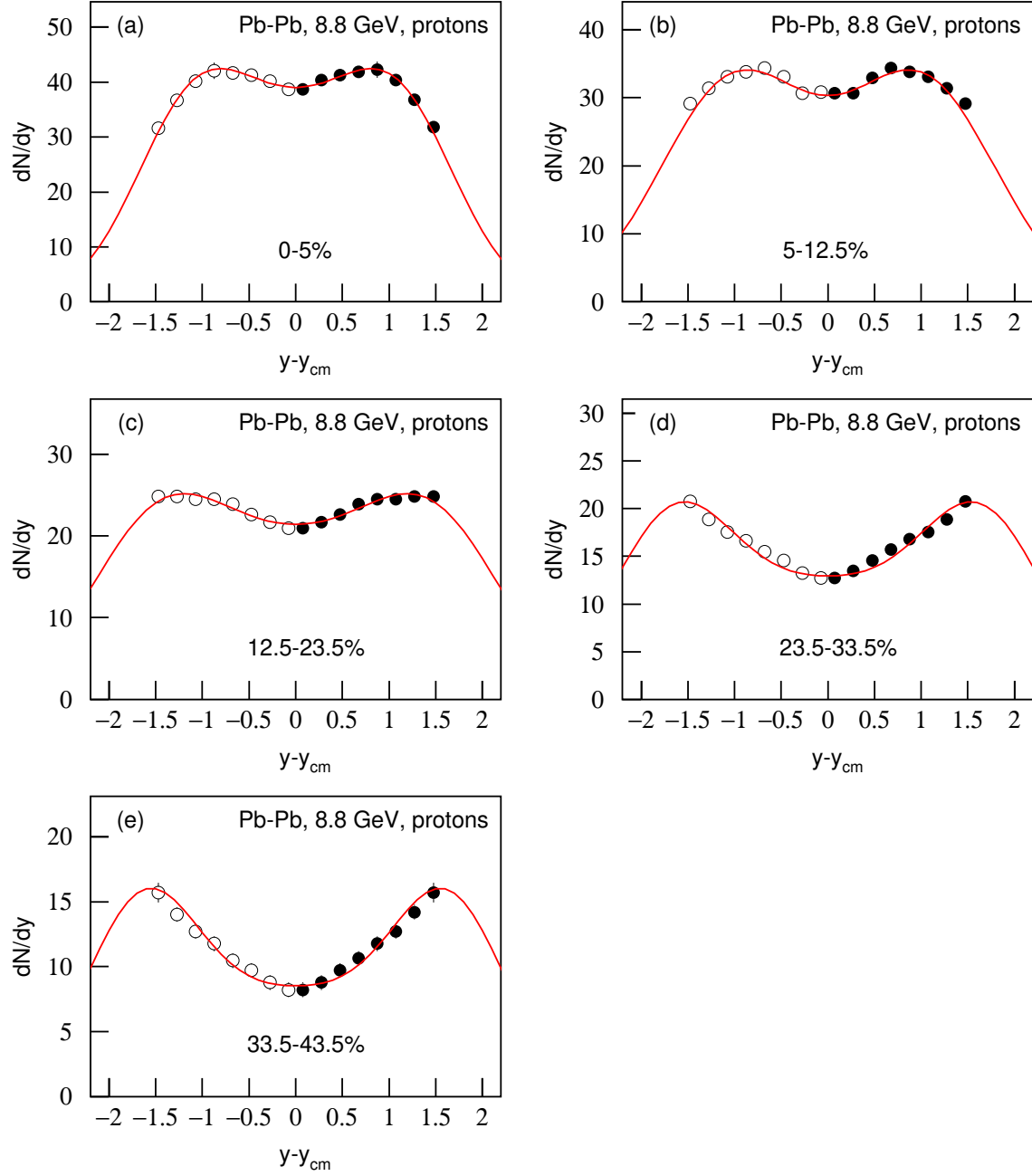


Figure 6. Rapidity distributions of protons emitted in Pb-Pb collisions at $\sqrt{s_{NN}} = 8.8$ GeV, where panels (a)–(d) correspond to centrality intervals 0–5%, 5–12.5%, 12.5–23.5%, and 23.5–33.5%, respectively. The closed circles represent the experimental data of the NA49 Collaboration [20] and the open circles are reflected at the mid-rapidity. The curves are our results fitted by the three-source distribution.

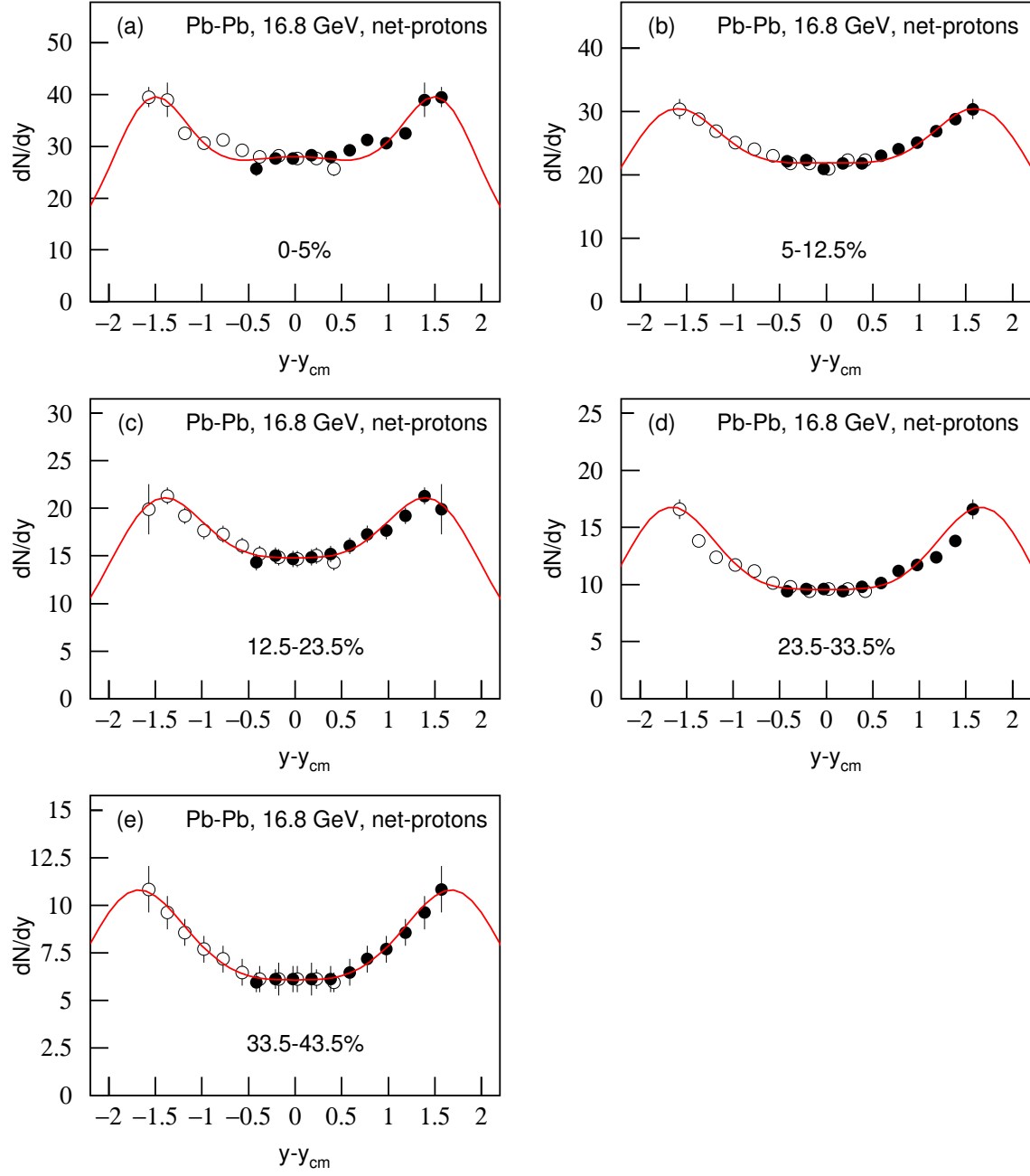


Figure 7. The same as Figure 6, but showing the results of net-protons emitted in Pb-Pb collisions at $\sqrt{s_{NN}} = 16.8$ GeV.

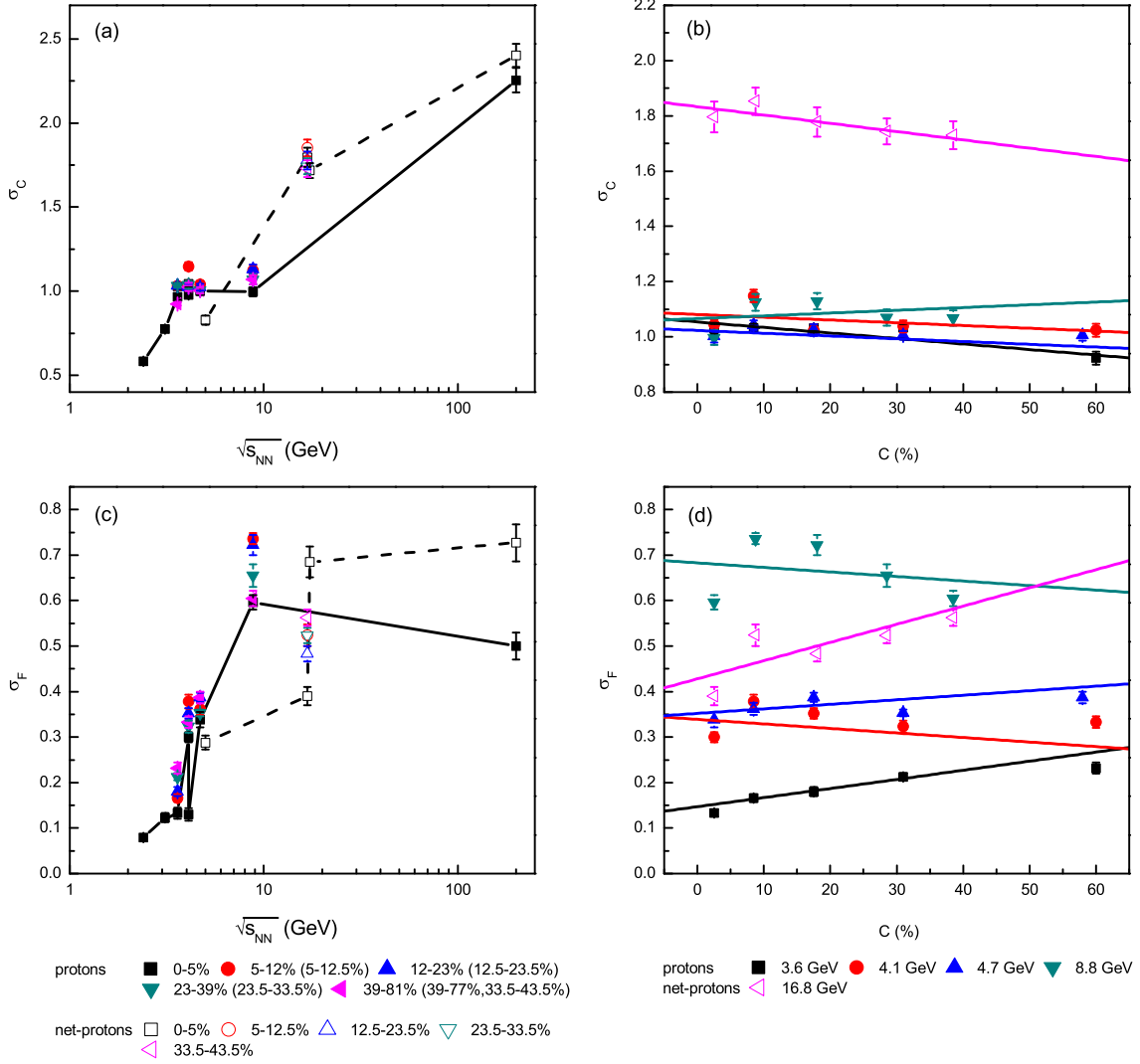


Figure 8. *Left:* Excitation functions of (a) σ_C , (c) σ_F , (e) k_C , and (g) Δy . Different symbols represent parameter values for different centrality intervals, where the closed and open symbols are from protons and net-protons respectively. The line segments in Figures 8(a) and 8(c) for central collisions are used to guide the eyes. Only the results for central collisions are presented in Figures 8(e) and 8(g) for the purpose of clarity and concision. The lines in Figure 8(g) are our results fitted by linear functions. *Right:* Dependences of (b) σ_C , (d) σ_F , (f) k_C , and (h) Δy on the centrality C . Different symbols represent parameter values for different energies, where the closed and open symbols are from protons and net-protons respectively. The lines in Figures 8(b), 8(d), and 8(f) are our results fitted by linear functions. The line segments in Figure 8(h) are used to guide the eyes.

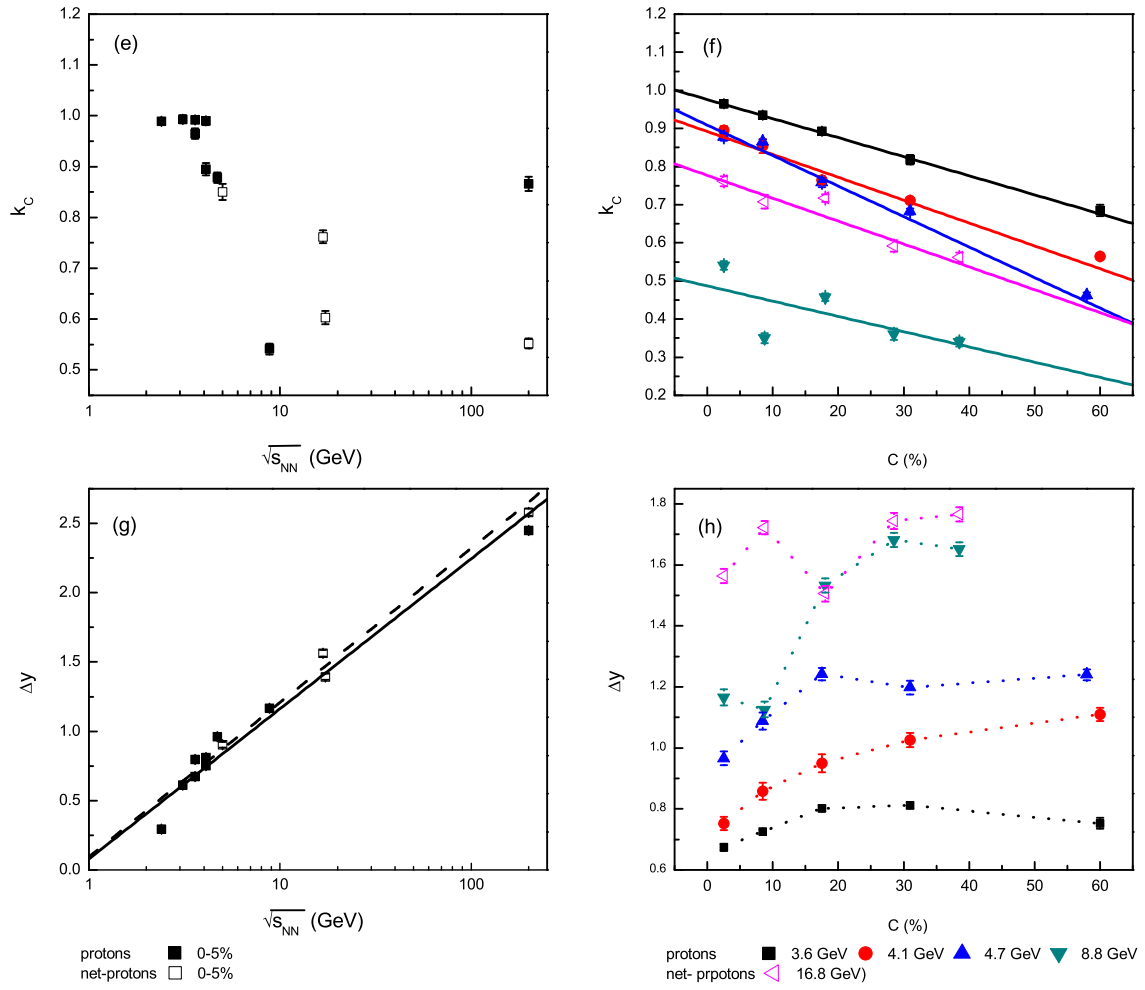


Figure 8. Continued.

the rapidity shift of (net-)protons are mainly determined by the collision energy. At or near the minimums, less Δy in central collisions renders larger viscosity due to more participant nucleons in the collisions. The decrease trend of k_C on C renders that multi-scattering results in more non-leading protons in central collisions than in peripheral collisions. The leading protons and their number determine both the rapidity shift and fraction in given central and forward (backward) rapidity regions.

We would like to point out that the parameters σ_C (σ_F) and Δy are generally independent of, and the parameter k_C is dependent on, the types of protons and net-protons. In particular, in Figure 8(e), there are a few points which are taken from the rapidity distributions of net-protons at $\sqrt{s_{NN}} = 5, 16.8, 17.3$, and 200 GeV, which give smaller k_C than that from protons and do not affect our main conclusion on the dependence of k_C on $\sqrt{s_{NN}}$. If all of the points at $\sqrt{s_{NN}} = 5, 16.8, 17.3$, and 200 GeV are taken from protons, we expect a higher saturation value (> 0.70) for k_C at $\sqrt{s_{NN}} > 17$ GeV. In Figure 8(f), the points at $\sqrt{s_{NN}} = 16.8$ GeV are taken from net-protons, which show a similar law as those taken from protons at lower energies.

The present work confirms one of our recent works [16] in which the method of squared speed-of-sound analysis is used according to the widths of rapidity distributions of negatively charged pions, and the minimum is observed at $\sqrt{s_{NN}} = 8.8$ GeV. The present work also confirms another recent work of ours [23] in which the method of string tension analysis is used due to the Schwinger mechanism description of transverse momentum distribution of identified particles, and the minimum is observed at $\sqrt{s_{NN}} = 7.7$ GeV.

The present work is consistent with other works. For example, refs. [24, 25] indicated the minimum locating in $\sqrt{s_{NN}}$ range from 4 to 9 GeV, in which the Landau hydrodynamic model and the ultra-relativistic quantum molecular dynamics hybrid approach are used. A wiggle in the excitation function of a specific reduced curvature of the net-proton rapidity distribution at midrapidity is expected in the $\sqrt{s_{NN}}$ range from 4 to 8 GeV [4–6]. Other works which study the excitation functions of mean transverse mass minus rest mass [26], chemical freeze-out temperature [26, 27], yield ratios of positive kaons to pions [26–28], and width ratios of experimental negative pion rapidity distribution to Landau hydrodynamic model prediction [27] show a knee point around $\sqrt{s_{NN}} = 7$ –8 GeV.

It is hard to connect the minimums of the model parameters with the softest points of the EoS, because the three-source distribution used in the present work does not consider the system evolution and the EoS. Various minimums extracted from different excitation functions may be different. To search for the minimal minimum, we have to extract the minimums of the excitation functions of the parameters in many distributions and correlations which include, but are not limited to, the rapidity distribution, transverse momentum spectrum, multiplicity distribution, transverse energy spectrum, fragmentation function distribution, dependences of anisotropic flow on rapidity and transverse momentum, and anisotropic flow distribution. This is a huge project which is beyond the scope of the present work.

It should be noted that, in our previous works [14–16], the width of rapidity distribution of newly produced particles is used to extract the squared speed-of-sound parameter based on the Landau hydrodynamic model [29–31]. Protons and net-protons are not newly produced particles. They are confined by the baryon conservation. Strictly speaking, the (net-)protons are beyond the scope of the Landau hydrodynamic model. In fact, this

model does not consider the continuity equation for baryon charge conservation. Therefore, the width of rapidity distribution of (net-)protons discussed in the present work should not be used to extract the squared speed-of-sound parameter.

4 Conclusions

We summarize here our main observations and conclusions.

a) The rapidity distributions of protons and net-protons emitted in Au-Au and Pb-Pb collisions over a $\sqrt{s_{NN}}$ range from 2.4 to 200 GeV are analyzed by using the three-source distribution. The model results can fit the experimental data of a few collaborations who worked at the AGS, SPS, and RHIC, respectively. Some interesting trends of parameters on energy are obtained.

b) The rapidity distribution width σ_C for the central rapidity region increases generally with increase of $\sqrt{s_{NN}}$. The trend of general increase in σ_C renders a continuous expansion of the central rapidity region in the considered energy range. The rapidity distribution width σ_F for the forward/backward rapidity regions increases initially with increase of $\sqrt{s_{NN}}$ and then saturates at above 8.8 GeV and fluctuates around its value at 17 GeV. The saturation of σ_F renders the nuclear limiting fragmentation in the forward/backward rapidity regions.

c) With increasing $\sqrt{s_{NN}}$, k_C decreases quickly from 0.98 at 2.1 GeV to 0.55 at 8.8 GeV, and saturates to about 0.70 at above 17 GeV. This renders that k_C has a minimum at $\sqrt{s_{NN}} = 8.8$ GeV. The saturation of k_C renders that the number of non-leading protons which stay in the central rapidity region is independent of energy at $\sqrt{s_{NN}} > 17$ GeV. In the considered energy range, Δy increases linearly with increase of $\ln(\sqrt{s_{NN}})$, which reflects the power of nuclear penetration which also increases with increase of $\ln(\sqrt{s_{NN}})$.

d) The minimum in the excitation function of k_C obtained in the present work confirms one of our recent works [16] in which the minimum is observed at $\sqrt{s_{NN}} = 8.8$ GeV by using the method of squared speed-of-sound analysis on the widths of rapidity distributions of negatively charged pions. The present work also confirms another recent work ours [23] in which the minimum is observed at $\sqrt{s_{NN}} = 7.7$ GeV by using the method of string tension analysis in the Schwinger mechanism on the transverse momentum distribution of identified particles.

e) Mainly for the considered five energies, σ_C and σ_F have a slight change or do not change with decrease of the centrality (or increase of the centrality percentage). With decrease of the centrality, Δy increases for the energies at or near the minimums, and does not change obviously for the energies apart from the minimums. The near independences of σ_C (σ_F) and partly Δy from centrality render that the rapidity shift of (net-)protons are mainly determined by the collision energy. At or near the minimums, less Δy in central collisions renders larger viscosity due to more participant nucleons in the collisions.

f) With decrease of the centrality, k_C decreases conformably for the five energies. The decrease trend of k_C on centrality renders that multi-scattering results in more non-leading protons in central collisions than in peripheral collisions. The leading protons and their number determine both the rapidity shift and fraction in given central and forward

(backward) rapidity regions.

Conflict of Interests

The authors declare that there is no conflict of interests regarding the publication of this paper.

Acknowledgments

This work was supported by the National Natural Science Foundation of China under Grant No. 11575103 and the US DOE under contract DE-FG02-87ER40331.A008.

References

- [1] EMU-01 Collaboration (M.I. Adamovich et al.), Phys. Lett. B **201**, 397 (1988).
- [2] K.K. Olimov, Q. Ali, M.Q. Haseeb, A. Arif, S.L. Lutpullaev, B.S. Yuldashev, Int. J. Mod. Phys. E **24**, 1550049 (2015).
- [3] Z.J. Jiang, J. Wang, Y. Huang, Int. J. Mod. Phys. E **25**, 1650025 (2016).
- [4] Y.B. Ivanov and D. Blaschke, Phys. Rev. C **92**, 024916 (2015).
- [5] Y.B. Ivanov, Phys. Lett. B **721**, 123 (2013).
- [6] Y.B. Ivanov, Phys. Rev. C **87**, 064904 (2013).
- [7] BRAHMS Collaboration (I.G. Bearden et al.), Phys. Rev. Lett. **93**, 102301 (2004).
- [8] R.A. Lacey, Phys. Rev. Lett. **114**, 142301 (2015).
- [9] NA49 Collaboration (S.V. Afanasiev et al.), Phys. Rev. C **66**, 054902 (2002).
- [10] NA49 Collaboration (C. Alt et al.), Phys. Rev. C **77**, 024903 (2008).
- [11] G. Wolschin, Eur. Phys. J. A **5**, 85 (1999).
- [12] G. Wolschin, J. Phys. G **40**, 045104 (2013).
- [13] G. Wolschin, Prog. Part. Nucl. Phys. **59**, 374 (2007).
- [14] L.-N. Gao, F.-H. Liu, Adv. High Energy Phys. **2015**, 184713 (2015).
- [15] L.-N. Gao, F.-H. Liu, Adv. High Energy Phys. **2015**, 641906 (2015).
- [16] F.-H. Liu, L.-N. Gao, R.A. Lacey, Adv. High Energy Phys. **2016**, 9467194 (2016).
- [17] E917 Collaboration (B.B. Back et al.), Phys. Rev. Lett. **86**, 1970 (2001).
- [18] E895 Collaboration (J.L. Klay et al.), Phys. Rev. Lett. **88**, 102301 (2002).
- [19] F. Videbæk, Nucl. Phys. A **830**, 43c (2009) (for the BRAHMS collaboration).
- [20] NA49 Collaboration (T. Anticic et al.), Phys. Rev. C **83**, 014901 (2011).
- [21] M. Murray, J. Phys. G **31**, S1137 (2005) (for the BRAHMS Collaboration).
- [22] F.-H. Liu, Mod. Phys. Lett. A **23**, 337 (2008).
- [23] L.-N. Gao, F.-H. Liu, R.A. Lacey, Eur. Phys. J. A **52**, 137 (2016).
- [24] M. Bleicher, arXiv: hep-ph/0509314 (2005).

- [25] J. Steinheimer, M. Bleicher, Eur. Phys. J. A **48**, 100 (2012).
- [26] L. Kumar, J. Phys. G **38**, 124145 (2011) (for the STAR Collaboration).
- [27] A. Rustamov, Cent. Eur. J. Phys. **10**, 1267 (2012).
- [28] D.T. Larsen, J. Phys. Conf. Ser. **668**, 012020 (2016).
- [29] L.D. Landau, *Collected Papers of L. D. Landau*, D. Ter-Haarp (Ed.), p. 569, Pergamon, Oxford, UK (1965).
- [30] E.V. Shuryak, Yadernaya Fizika **16**, 395 (1972).
- [31] P. Carruthers, Annals of the New York Academy of Sciences **229**, 91 (1974).